

ORIGINAL RESEARCH ARTICLE

Molecular docking and molecular dynamic of new thioguanine derivatives as histone deacetylase inhibitors

Mustafa M. Mukhlif^{1,*}, Ameer H. Alwash¹, Saraa M. Harbi¹, Shymaa A. Husein², Mohammed Khalid Abbood³, Hind A. Yaseen⁴

¹ Department of Pharmaceutical Chemistry, College of Pharmacy, Al-Bayan University, 10011, Iraq

² Department of Pharmacy, Al-Nukhba University Collage, 10011, Iraq

³ Department of Clinical Pharmacy, College of Pharmacy, Al-Bayan University, 10011, Iraq

⁴ Ibn Sina University of Medical and Pharmaceutical Sciences, 10011, Iraq

*Corresponding author: Mustafa M. Mukhlif, Mustafa.mo@albayan.edu.iq

ABSTRACT

Histone deacetylase inhibitors (HDAC-I) comprise structurally diverse molecules that are a group of targeted anticancer agents. Thioguanine is Purine derivatives used for acute myeloid leukemia treatment. A five new proposed analogs of thioguanine was investigated through molecular docking simulation to assess their binding affinity and therapeutic activity. Molecular dynamic (MD) modeling was conducted for 100 nanoseconds (ns) to investigate the molecular stability of the proposed compounds with the best docking results with histone deacetylase-2 (HDAC-2) and histone deacetylase-8 (HDAC-8) binding pocket. Root mean square deviation (RMSDs) for the ligands and complexes concerning their initial locations inside the active site has been reported and examined. Lastly, a thorough analysis and evaluation of the interactions between proposed analogs was also performed. The core tetrahedral carbon atom of an amino acid alpha carbon (C α) in the protein was used to track the conformational stability of the protein structures to their starting positions. 2-(4-(((6-thioxo-6,7-dihydro-3H-purin-2-yl)imino)methyl)benzoyl)hydrazine-1-carboxamide Compound 2/HDAC-8 complex showed some major fluctuations during simulation time at 17-19 ns; the ligand simulation fluctuated was found to be 4.5 angstroms (Å), and the protein skeleton fluctuated within 2 Å. 2-(4-(((6-thioxo-6,7-dihydro-3H-purin-2-yl)imino)methyl)benzoyl)hydrazine-1-carboxamide Compound 2/HDAC-2 The complex's RMSD value was within 1.80 Å, indicating good stability inside the target pocket.

Keywords: histone deacetylase; thioguanine; purine analogs; molecular docking; molecular dynamic.

ARTICLE INFO

Received: 23 August 2025

Accepted: 09 December 2025

Available online: 16 December 2025

COPYRIGHT

Copyright © 2025 by author(s).

Applied Chemical Engineering is published by Arts and Science Press Pte. Ltd. This work is licensed under the Creative Commons Attribution-NonCommercial 4.0 International License (CC BY 4.0).

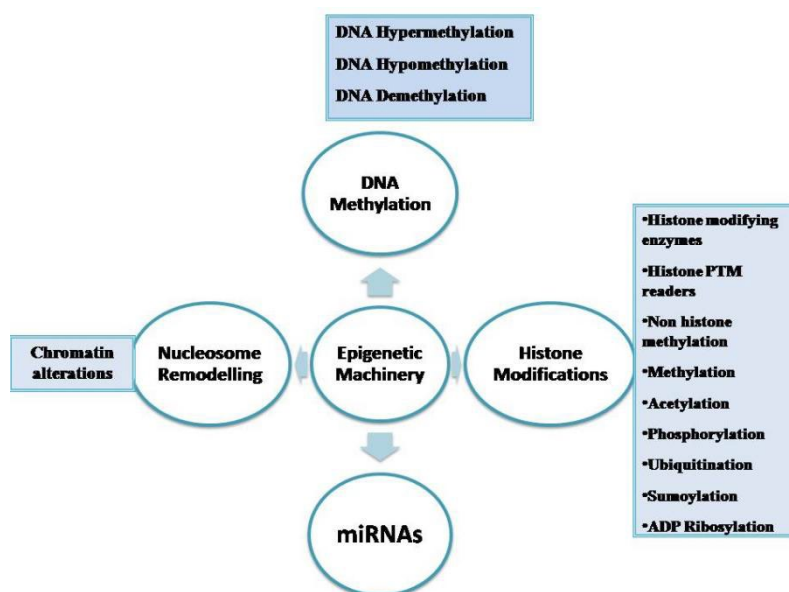
<https://creativecommons.org/licenses/by/4.0/>

1. Introduction

Epigenetics refers to inheritable modifications in gene expression that occur without changes to the DNA sequence.¹ all human cancers develop due to epigenetic alterations that regulate inheritable changes. (Table 1, Figure 1). Epigenetic modifications include alterations in chromatin composition and structure, abnormal DNA methylation patterns, and disruptions in histone post-translational modifications (PTMs) Disrupted epigenetic machinery is primarily responsible for these epigenome alterations. DNA is wrapped around histones in a nucleosome to constitute the epigenetic apparatus. Mutations in signaling genes, or oncogenes, are frequently prevalent in a significant proportion of human tumors and are responsible for the development of cancers.^[2,3]

Table 1. Samples of epigenetic modulation in altered human cancerous cellular pathways.

Pathway	Epigenetic Alteration	Role of Epigenetic Alteration
Self-sufficiency and self-dependent for growth event related signals	Methylation of RASSF1A gene	Loss of tumor suppressor activity
Not sensitive to antigrowth related signals	Down-regulation of TGF- β receptors	Reduces responsiveness to growth inhibitory signals
Tissue invasion and metastasis related events	Methylation of E-cadherin promoter	Decreases cell adhesion, facilitating metastasis
Unlimited replication capacity	Silencing of p16 or pRb genes by promoter methylation	Disruption of cell cycle control, enabling unlimited divisions
Continuous angiogenesis and related cellular pathways	Silencing of thrombospondin-1	Promotes new blood vessel formation for tumor growth
Strength to evade apoptosis	Methylation of DAPK, ASC/TMS1, and HIC1	Inhibits programmed cell death, aiding in tumor survival
Capacity to repair DNA	Methylation of GST Pi, O6-MGMT, MLH1	Disables DNA repair systems, leading to mutation accumulation
Genomic instability monitoring cellular pathways	Methylation of Chfr	Result in chromosomal instability and mitotic defects
Protein ubiquitination functions regulating mitotic control genes	Methylation of Chfr	block degradation of mitotic regulators, affecting cell cycle checkpoint control

**Figure 1.** The epigenetic machinery.^[2]

Histone acetylation is one known epigenetic alteration linked to the emergence of cancer and other illnesses. The two enzymes, histone acetyl transferase (HAT) and histone deacetylase (HDAC) dynamically modulate the acetylation of histone proteins^[4]. HDAC enzyme inhibition represents a promising strategy for anticancer therapy^[5]. The FDA has approved the use of vorinostat, panobinostat, belinostat, and romidepsin, as HDAC inhibitors for cancer treatment in combination with other antineoplastic agents or even as a monotherapy. Three HDAC inhibitors currently employed in clinical settings utilize the hydroxamate moiety as the zinc-binding group (ZBG). However, hydroxamate has been reported to exhibit poor pharmacokinetics and considerable toxicity.^[6]

In the 1940s and 1950s, various substances were formed with a potential objective of curing cancer^[7]. At that time, vitamins, later recognized as folates and purines, were recognized as essential for cellular survival and play a critical role in the synthesis of deoxyribonucleic acid (DNA). However, the metabolism of purines and folate was a mystery at the time.^[8] They reasoned that one way to destroy cancer cells would be to interfere

with the metabolism of purines and folate. Thus, they created analogues of purines and folate with the goal of obstructing DNA synthesis. Thioguanine (TG), a thiopurine derivative introduced in 1950, was among the first compounds shown to effectively inhibit the proliferation of leukemic cells.^[9] Afterward, other thiopurine derivatives, such as azathioprine (AZA) (1957) and mercaptopurine (MP) (1951), were created to increase therapeutic choices and were investigated for the treatment of inflammatory and immunological disorders. Over the past 70 years, thioguanine (TG) has undergone continuous refinement, repurposing, and reevaluation for the treatment of solid tumours, acute lymphoblastic leukaemia (ALL), acute myeloid leukaemia (AML), and chronic myeloid leukaemia (CML).^[10] (mostly in conjunction with other anti-cancer medications), but also for immune-mediated and inflammatory conditions. TG was first made available in 2001 as a potentially effective treatment option for inflammatory bowel disease (IBD) patients who had not responded to MP or AZA.^[11] Over the years, TG has also been investigated as a potential alternative therapy for autoimmune hepatitis and various hepatogastrointestinal conditions.^[12], complicated celiac disease^[13] or collagenous sprue^[14]. Additionally, TG has been employed in the fields of rheumatology and dermatology to treat certain conditions like systemic lupus erythematosus (SLE) and psoriasis.^[15] Our objective is to highlight the advantages of TG derivatives as HDAC inhibitors regarding the pharmacokinetic properties of the derivatives.

2. Materials and methods

2.1. Molecular docking

The investigated compounds' potential affinity for HDAC-2 (PDB ID: 4lxz) and HDAC-8 (PDB code: 1t69), which were taken from the protein data bank, was assessed using molecular docking. Initially, the compounds were cleared of water molecules. Subsequently, crystallographic abnormalities and empty valence atoms were prepared and corrected using the available choices. Via force fields, protein structural energy was reduced. The 2D structures of the compounds were generated using Chem-Bio Draw Ultra 16.0 and saved in SDF file format. Then, the file was opened, the 3D structures were protonated, and the 0.1 RMSD kcal/mole energy was reduced. The reduced structures were then ready for docking using the ligand preparation tools.^[16] The docking process was done through the docking option using Autodock Vina 1.5.7 software^[17] The ligands were allowed to remain flexible while the receptor was maintained in a rigid conformation. During the refinement process, each molecule was allowed to adopt twenty well-defined poses with the proteins. The Discovery Studio 2016 Visualizer was subsequently employed to produce 3D figures and report the docking scores (affinity energy) with poses that are best fitted with the active spots^[18].

2.2. Molecular dynamic (MD) simulation

Molecular dynamics (MD) simulations were conducted using Schrödinger LLC's Desmond software.^[19] The NPT ensemble was used consistently throughout all runs, with a temperature of 300 K and a pressure of 1 bar. The ligands under investigation underwent a relaxation time of 1 ps during the 100 ns simulations. The OPLS_2005 force field parameters were applied in each simulation. The Particle Mesh Ewald method was employed to compute long-range electrostatic interactions, with a Coulomb interaction cutoff radius set to 9.0 Å^[20]. The Simple Point Charge model was utilized to represent water molecules explicitly. Temperature control was managed using the Nosé–Hoover chain coupling method, while pressure control was achieved through the Martyna–Tuckerman–Klein chain coupling system, with a coupling constant of 2.0 ps. The r-RESPA integrator computed non-bonded forces, updating the long-range forces every three steps and the short-range forces at each step. Trajectories were saved at 4.8 ps intervals for later examination.

The Interaction Diagram tool in the Desmond MD package used for the simulation was utilized to examine the interactions and behavior between ligands and proteins. The reliability of MD simulations was assessed by tracking the RMSD of the locations of the ligand and protein atoms over time. Additionally, the AMBER 14 package (Case et al. 2008) was employed for numerous purposes, including minimization, counterion addition,

solvation, equilibration, and running periodic box simulations using explicit water (TIP4P) MD simulations for the investigated ligands. The AMBER force field ff99 was utilized for these simulations. The ligand structures were refined utilizing the B3LYP density functional theory (DFT) method with a 6-31G basis set, and the GAFF force field was applied to define the parameters. The protein-ligand-water system was given flexibility during simulations, which included ten separate runs with various random beginning velocities. Using a time-step of 0.001 ps (1 fs), each run lasted 10 ns. Compared to longer, single-trajectory simulations, these multiple MD simulations, which are widely accepted, could sufficiently sample conformational space. The AMBER Tools distribution's cpptraj software was used to analyze the data.

3. Results

3.1. HDAC-2 inhibition:

Analysis of how **Compound 1** binds to HDAC-2 exhibited an affinity score equal to -7.34 kcal/mol. **Compound 1** interacted with His183, Phe155, Phe210, and Leu276 by six hydrophobic π -interactions. Additionally, five hydrogen bonds (H-bonds) were found to support the interaction and two metal ionic interactions with Gly154, Gly306, His145, Tyr308, and Zn401 with distances of 1.92, 2.65, 2.76, 2.01, and 2.01.86 Å (**Figure 2**). Meanwhile, **compound 2** indicated an affinity score of -8.13 kcal/mol. It generated four hydrophobic π -interactions with Asp104, Phe155, and His183, also formed metal ionic interaction and four hydrogen bonds with Zn401, Gly143, His145, and Gly154 with distances of 2.06, 2.59, 2.66 and 2.67 Å (**Figure 3**).

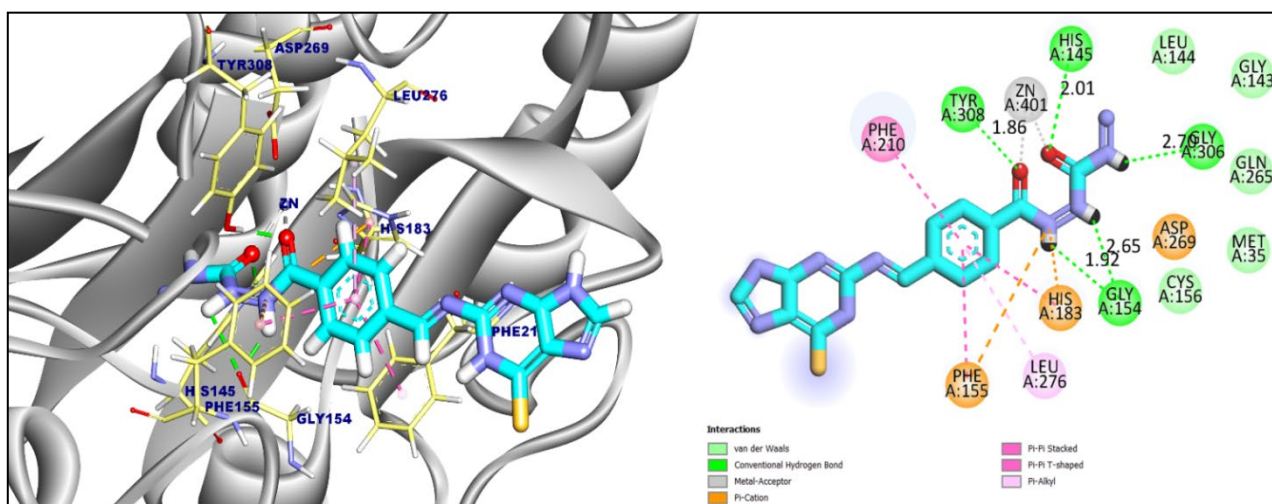


Figure 2. 3D figure of **Compound 1** against HDAC-2.

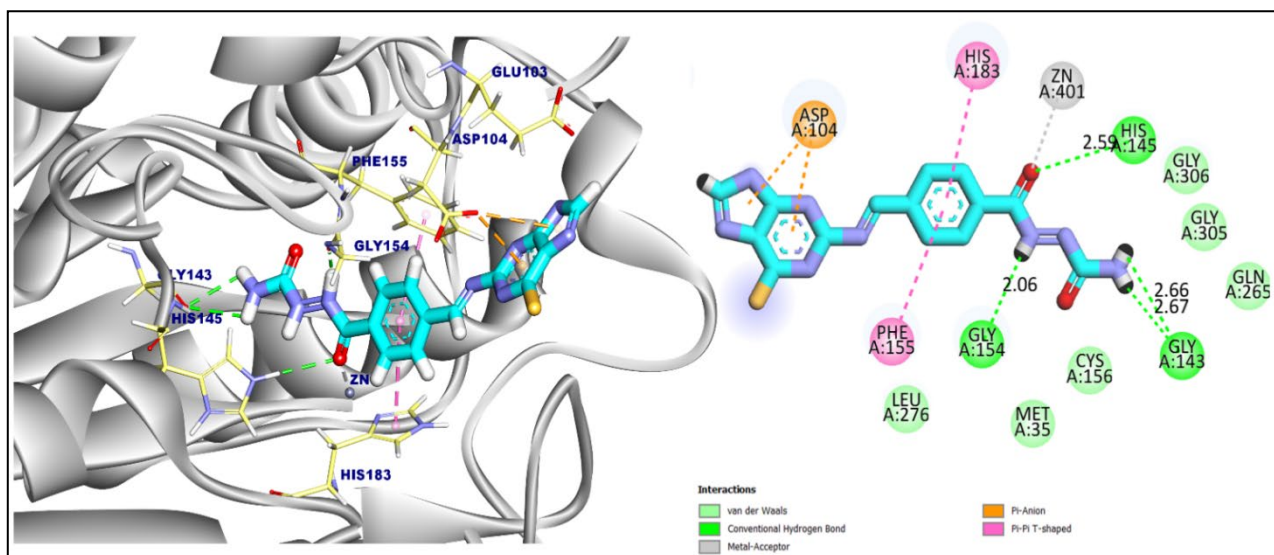


Figure 3. 3D and 2D figures of **Compound 2** against HDAC-2.

Compound 3 - HDAC-2 binding mode revealed binding energy equal to -5.63 kcal/mol, **Compound 3** interacted by eight hydrophobic π -interactions with Tyr209, Phe210, Leu276, His183, Tyr308, and Phe155; moreover, it also interacted with Gly154, His145, His146, His183, Asp269, and Zn401 by six H-bonds and 2.13, 2.08, 2.76, 3.37, 3.07, and 3.68 Å metal ion interaction distances (**Fig 4**). on the other hand, the predicted binding interaction of **compound 4** showed a score of -6.28 kcal/mol. **Compound 4** interacted by two hydrophobic π -interactions with Phe155 and Asp104, and the interaction was stabilized by three H-bonds and ionic metal interactions with Gly154, His145, Asp104, and Zn401. The distances were 2.00, 2.26, and 3.07 Å (**Figure 5**). The predicted binding interaction of **compound 5** showed an affinity score of -5.41 kcal/mol. **Compound 5** has the same binding mode as **compound 4**, which formed metal ion interaction with Zn401 and was bound by three hydrophobic π -interactions with Asp104 and Phe155. Additionally, two H-bonds were observed with Gly154 and His145, showing the distances of 2.03 and 2.27 Å (**Figure 6**).

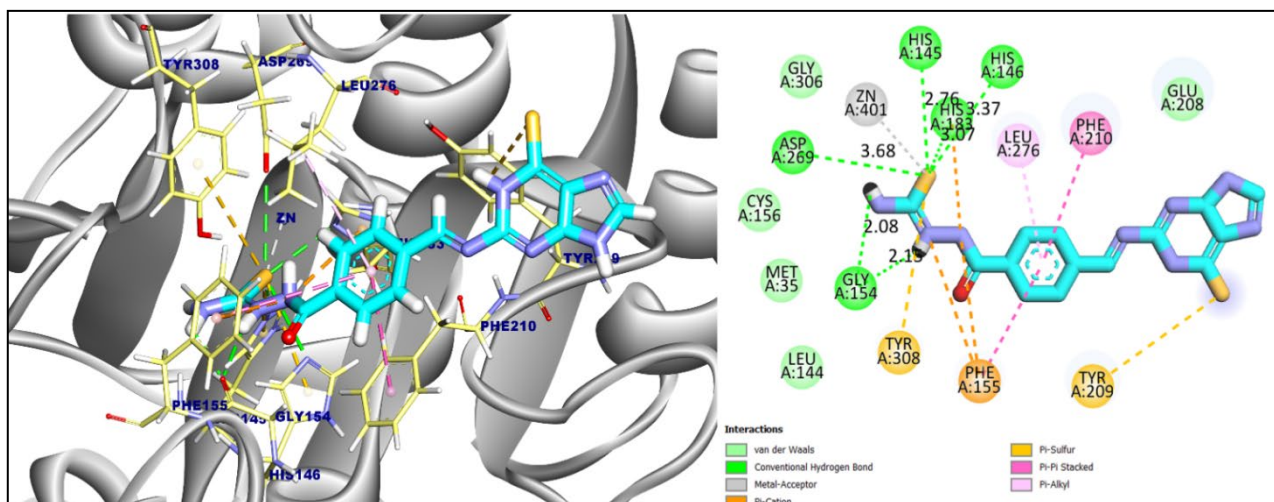


Figure 4. 3D figure of **Compound 3** against HDAC-2.

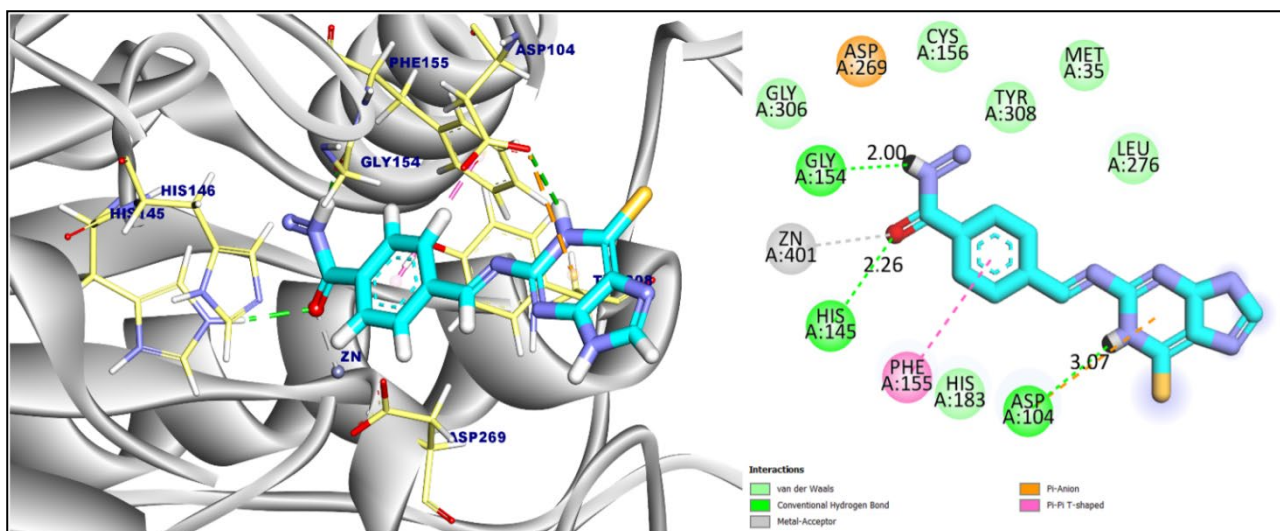


Figure 5. 3D figure of **Compound 4** against **HDAC-2**.

The reference drug (SAHA) complexed with HDAC-2, was redocked and showed an affinity score of -8.61 kcal/mol, which formed three hydrophobic π -interactions and metal ion bonds with Phe210, Phe155, Pro34, and Zn401. Additionally, it interacted with four H-bonds with His145, His146, Tyr308, and Asp104 with distances of 1.69, 1.67, 1.62, and 1.75 Å (**Figure 7**). The binding mode of the reference drug (Trichostatin) against **HDAC-2** exhibited an affinity score equal to -9.24 kcal/mol. Trichostatin interacted with His33, Pro34, Phe155, and Phe210 by seven hydrophobic π -interactions. Additionally, two hydrogen bonds were found to support the interaction along with two metal ionic interactions with His145, Tyr308, and Zn401, and the distance was found to be 1.82 and 2.05 Å (**Figure 8**).

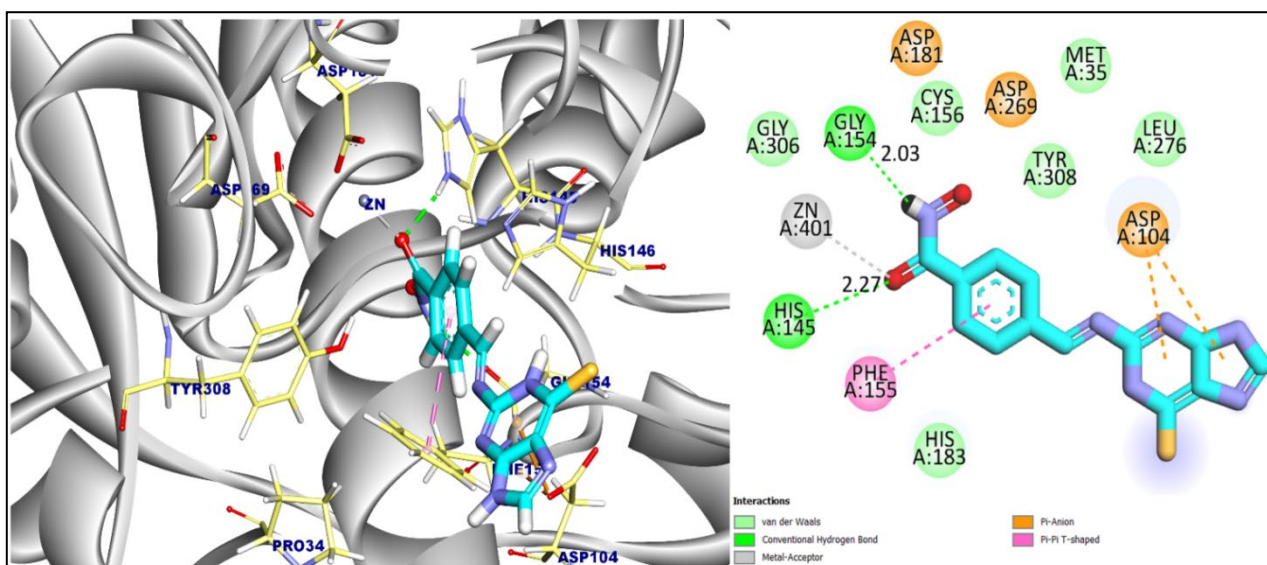


Figure 6. 3D figure of **Compound 5** against **HDAC-2**.

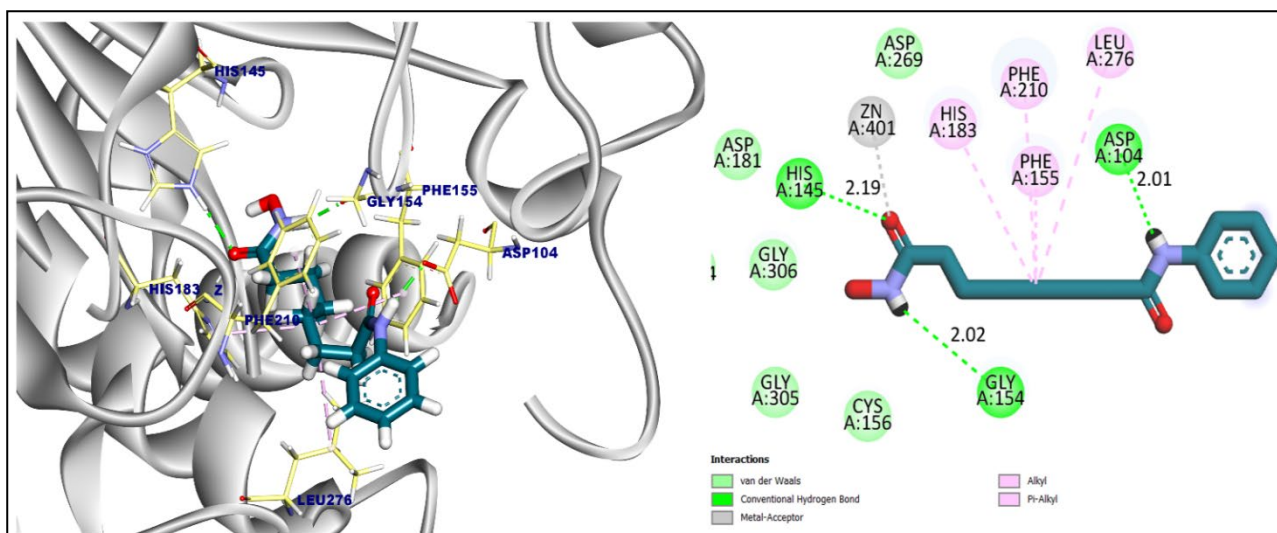


Figure 7. 2D and 3D representation of reference ligand binding (SAHA) with HDAC-2.

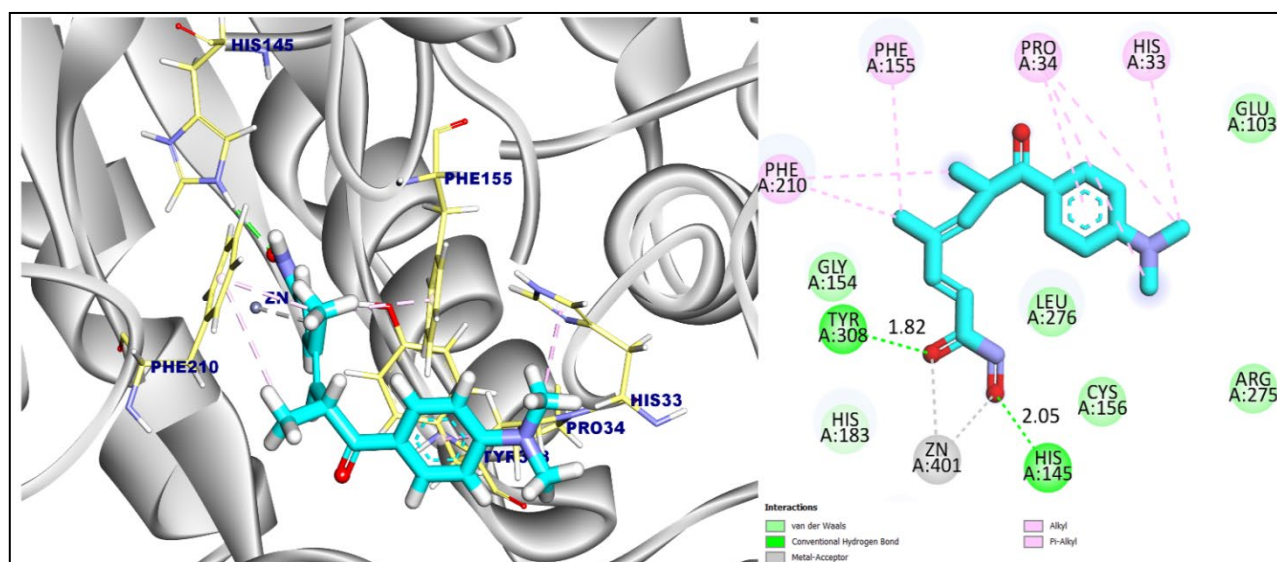


Figure 8. 2D and 3D representation of reference ligand binding (Trichostatin) with HDAC-2.

3.2. HDAC-8 inhibition:

The binding mode of **Compounds 1, 2, and 3** against HDAC-8 exhibited binding energies equal to -6.25, -7.93, and -5.05 kcal/mol, respectively. **Compound 1** formed four hydrophobic π -interactions and five H-bonds with Tyr100, Phe208, His180, Gly151, His143, Asp101, and Tyr306, respectively, with distances of 2.18, 2.31, 3.31, 3.08, and 2.62 Å, moreover, metal ionic bond was noted with Zn378 (**Fig 9**). additionally, compound 2 was interacted with Phe207, Met274, Phe208, Phe152, His180 and Zn378, through nine hydrophobic π -interactions and metal ionic bond. The interaction of compound 2 was facilitated by three H-bonds with His180 and Gly151 with distances of 2.83, 1.98, and 2.72 Å (**Figure 10**). While Compound 3 showed the same pattern of interaction as compound 2, it interacted with Lys202, Phe152, Phe208, Met274, His142, Tyr306, and Zn378 by ten hydrophobic π -interaction and ionic interaction. Furthermore, five H-bonds were identified with Gly151, His143, His180, and Asp178 with distances of 2.19, 2.25, 2.59, 3.01, and 2.78 Å (**Figure 11**).

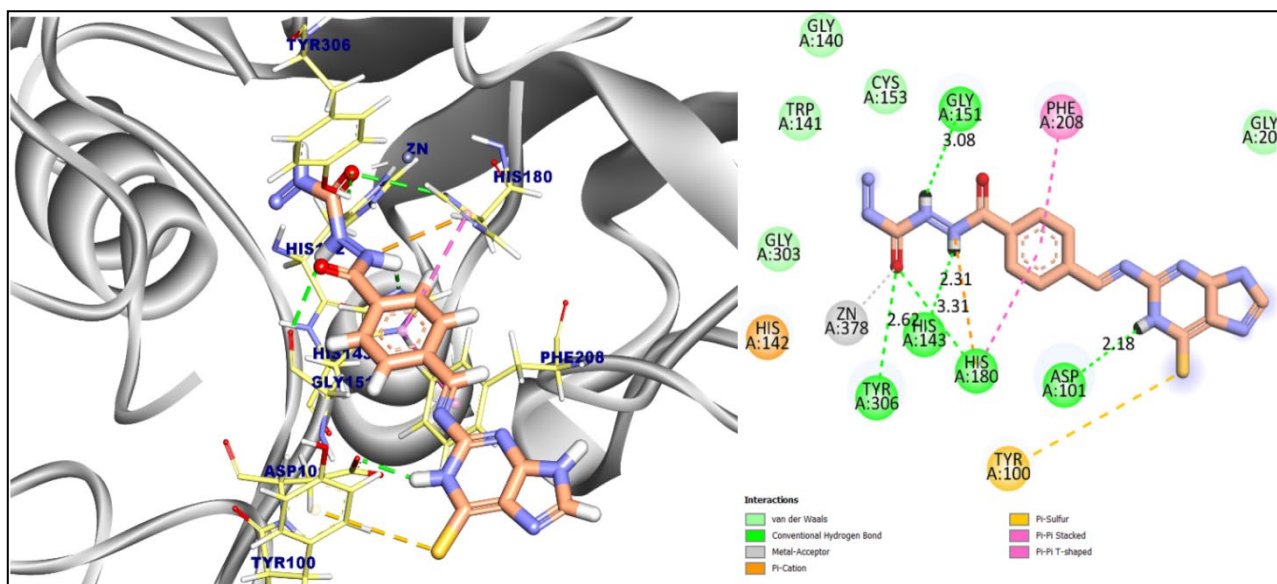


Figure 9. 3D and 2D representation of Compound 1 binding with HDAC-8.

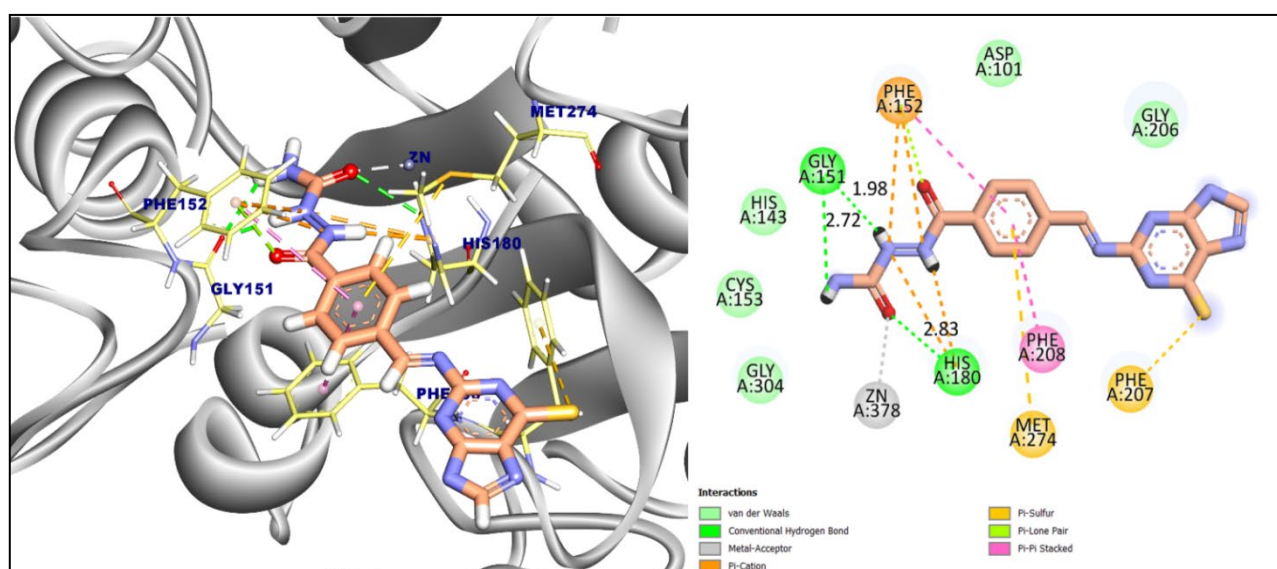


Figure 10. 2D and 3D representation Compound 2 binding with HDAC-8.

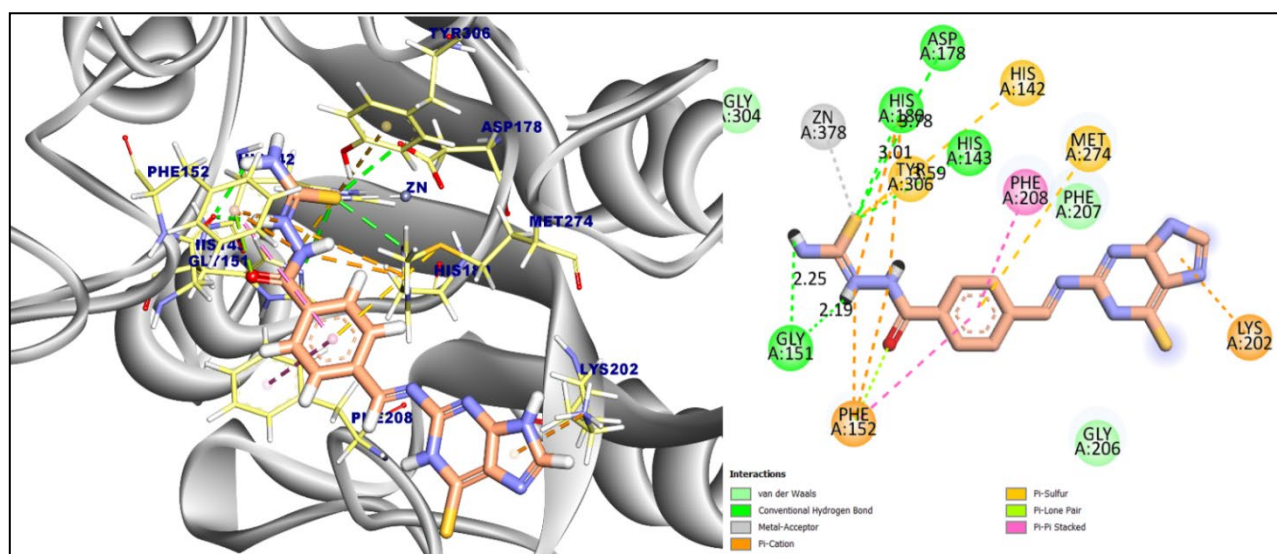


Figure 11. 2D and 3D representation Compound 3 binding with HDAC-8.

The predicted interaction of **Compound 4** presented a binding score of -5.95 kcal/mol. **Compound 4** was connected by six hydrophobic π -interactions and three hydrogen bonds with Phe207, Tyr306, Phe152, Phe208, His180, Asp101, and Trp141 with distances of 2.00, 1.99 and 2.39 Å and the interaction was supported by ionic metal interaction with Zn378 (**Figure 12**). Meanwhile, the proposed binding interaction of **compound 5** showed an affinity score of -5.60 kcal/mol. **Compound 5** developed metal ion interaction with Zn378 and interacted by four hydrophobic π -interactions with Tyr100, His180, and Phe152. Additionally, two H-bonds were observed with Gly151 and Asp101 showing distances of 1.86 and 2.60 Å (**Figure 13**).

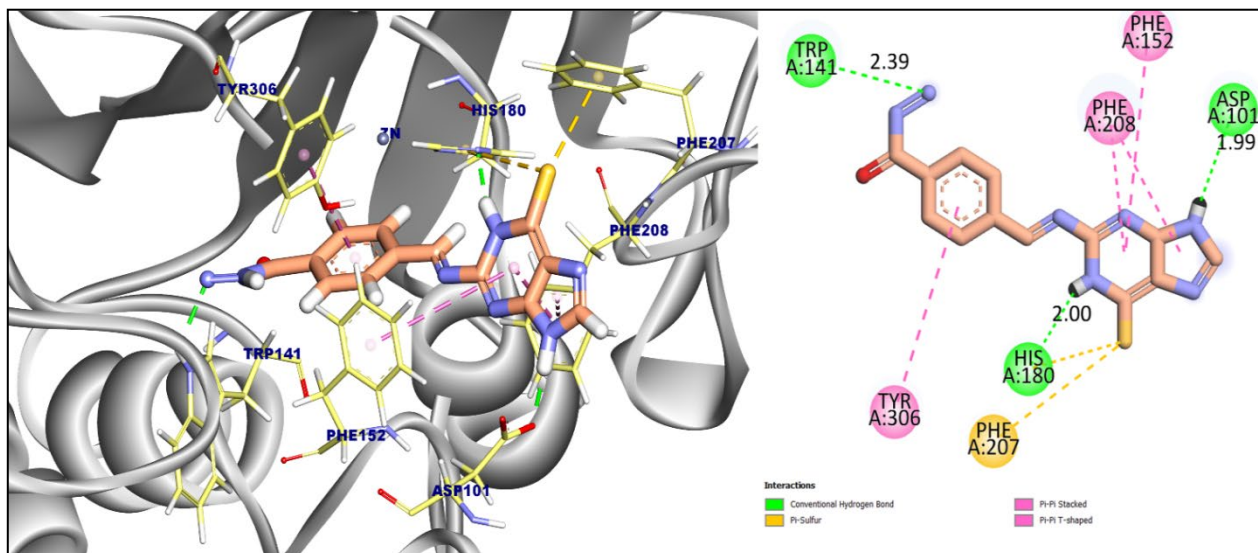


Figure 12. 2D and 3D representation Compound 4 binding with **HDAC-8**.

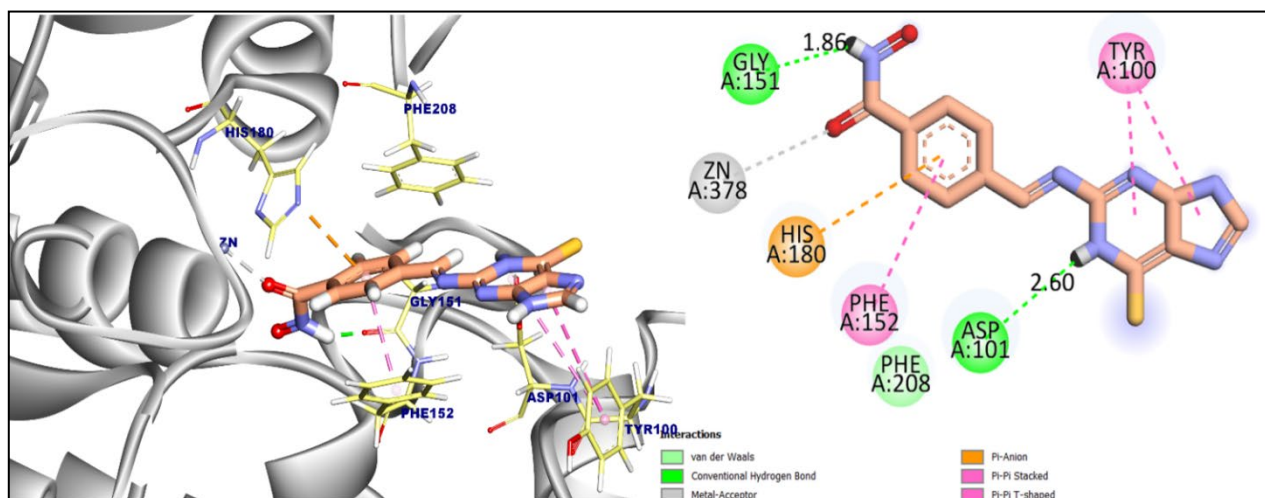


Figure 13. 3D and 2D representation Compound 5 binding with **HDAC-8**.

The reference compound (SAHA) against **HDAC-8** showed an binding score of -6.37 kcal/mol. which formed three π - hydrophobic bonds and metal ion interaction with Phe208, Phe152, His180, and Zn378, furthermore interacted with Phe208, Gly151, and His180 by three H-bonds with distances of 2.22, 1.92 and 2.85 Å (**Figure 14**).

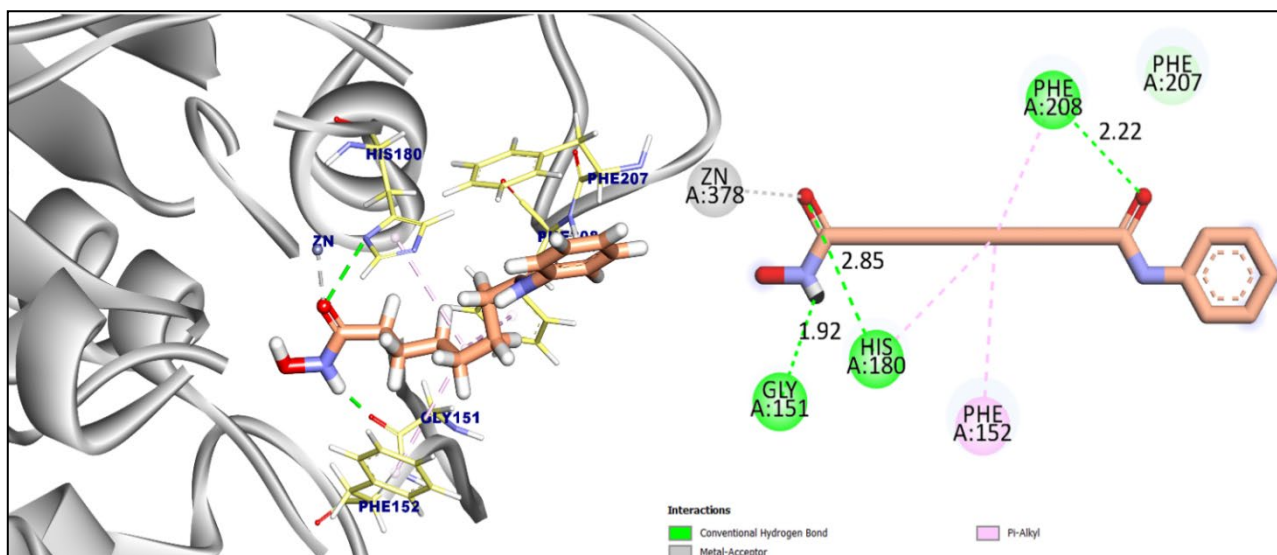


Figure 14. 2D and 3D representation of reference ligand binding (SAHA) with **HDAC-8**

The binding mode of the reference drug (Trichostatin) against HDAC-8 showed a binding score equal to -6.54 kcal/mol. Trichostatin interacted with Phe208, His180, Asp178, and Zn378 by two hydrophobic π -interactions and metal-ionic interactions. Additionally, the establishment of the interaction was established through forming three hydrogen bonds with His180, His142, and Gly151, and the distances were found to be 2.85, 2.26, and 2.57 Å (**Figure 15**).

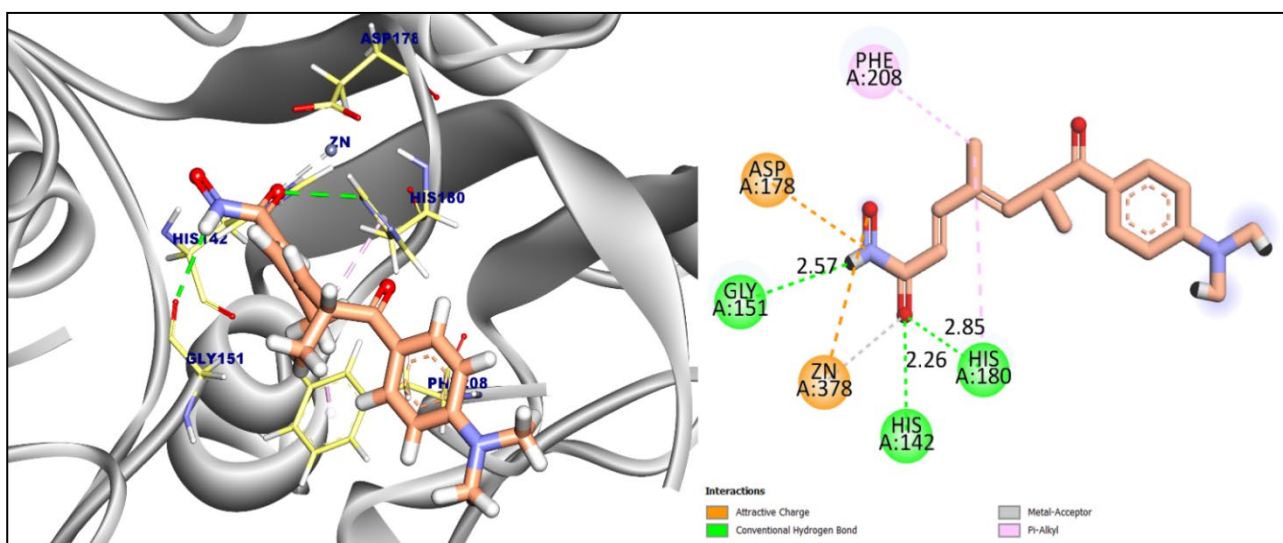
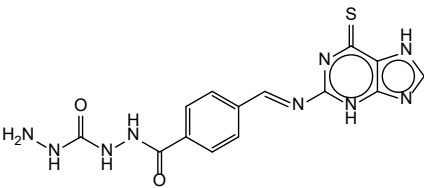
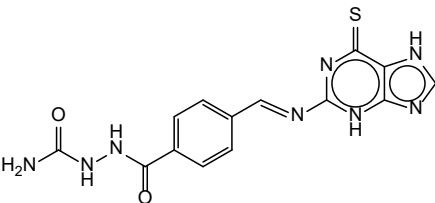
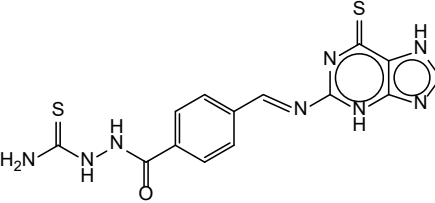
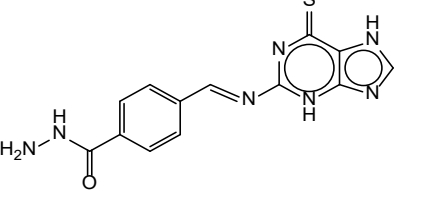
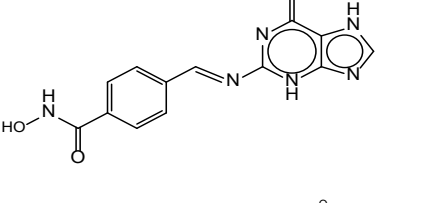
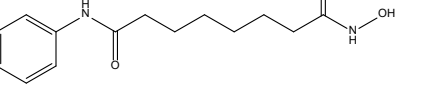
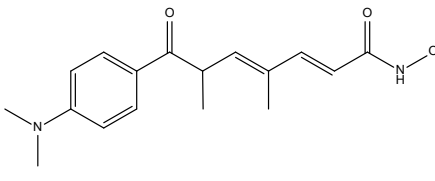
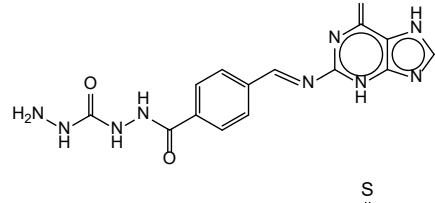
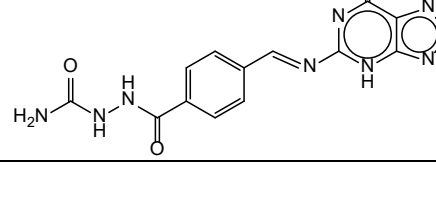


Figure 15. 2D and 3D representation of reference ligand binding (Trichostatin) with **HDAC-8**.

Table 2. The molecular docking results of the tested Compounds against **HDAC-2** and **HDAC-8**.

Target protein	Tested compounds	Compound Structure	RMSD value (Å)	Docking (Affinity) score (kcal/mol)
HDAC-2	Compound 1		1.42	-7.34

Target protein	Tested compounds	Compound Structure	RMSD value (Å)	Docking (Affinity) score (kcal/mol)
HDAC-8	Compound 2		1.98	-8.13
	Compound 3		1.85	-5.63
	Compound 4		1.83	-6.28
	Compound 5		1.76	-5.41
	SAHA		1.03	-8.61
	Trichostatin		1.76	-9.24
	Compound 1		0.95	-6.25
	Compound 2		1.99	-7.93

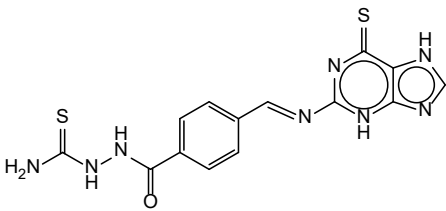
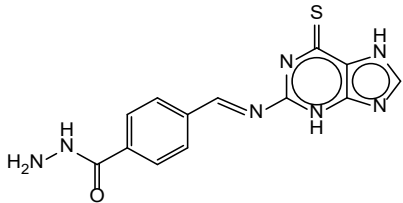
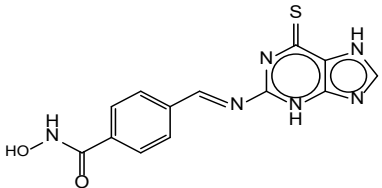
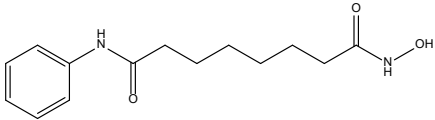
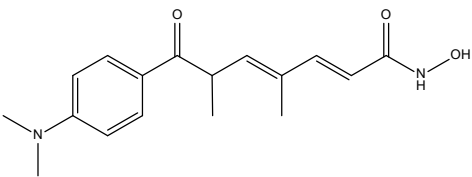
Target protein	Tested compounds	Compound Structure	RMSD value (Å)	Docking (Affinity) score (kcal/mol)
	Compound 3		1.74	-5.05
	Compound 4		1.38	-5.95
	Compound 5		1.49	-5.60
	SAHA		1.54	-6.37
	Trichostatin		1.76	-6.54

Table 2. (Continued)

3.3. Molecular dynamic (MD) simulation study

The molecular stability among the studied compounds showing the best docking results with the HDAC-2 and HDAC-8 binding pocket was investigated using 100 ns MD simulations. We reported and examined the ligands' and complexes' obtained root mean square deviations (RMSDs) with respect to their initial locations inside the active site. Lastly, a thorough analysis and evaluation of the interactions between Frontier substances was also conducted.

3.3.1. Enzyme-ligand RMSD and RMSF analysis

For MD simulation, compound 2, which was complexed with HDAC-2 and HDAC-8, was used. The protein's C α atoms were used to track the conformational stability of the protein structures with respect to their starting positions. The compound 2/HDAC-8 complex, as seen in Figures 16C and 16D, exhibited some significant fluctuations during the simulation period at 17–19 ns, demonstrating that the amino acid ligand interaction region had numerous conformational transformations. The simulation of the ligand fluctuated within 4.5 Å, while the fluctuation of the protein skeleton was found to be within 2 Å, suggesting that the ligand was not always stable in the interior of the target tunnel during the run of the simulation. The binding pattern of Compound 2 with the HDAC-8 binding site (**Figure 16D**) may be impacted by the changes in the HDAC-8 protein structure around the 30–40, 80–90, and 190–210 amino acid regions. Conversely, the Compound 2/HDAC-2 complex demonstrated excellent stability within the target tunnel, leading to an

acceptable RMSD value of 1.80 Å below 3.00 Å. Compound 2 exhibited stability throughout the simulation period, except for a slight fluctuation between 20 and 30 ns. Furthermore, the HDAC-2 protein structure fluctuated within 0.4 Å and demonstrated remarkable stability during the simulation period with few undesired conformational changes.

Moreover, it showed a minor fluctuation at 80-90 amino acids area, that indicate a few conformational changes occur and these changes do not have any effect on the ligand binding inside the active site **Figure 16a-b**.

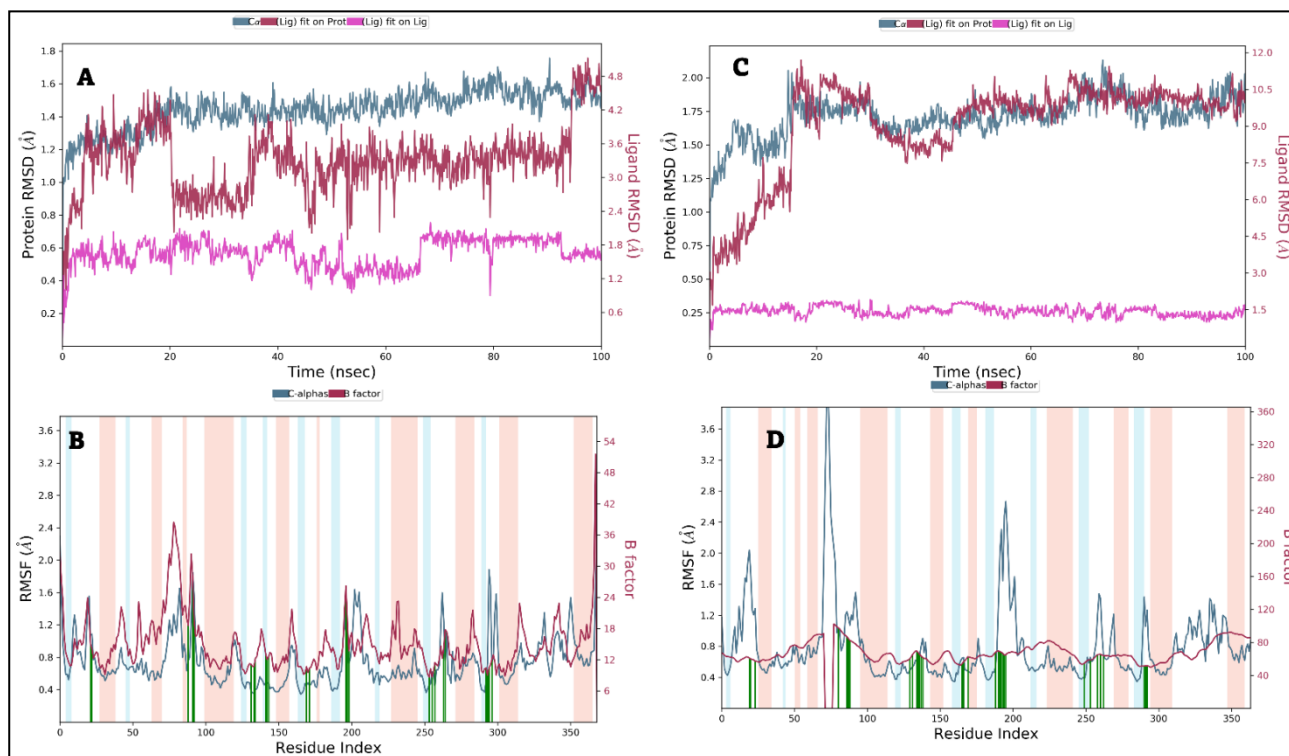


Figure 16. Explain the RMSD and RMSF of Compound 2 against HDAC-2 **16a-b** and against HDAC-8 **16c-d** over 100 ns.

3.3.2. Analysis of enzyme-ligand interaction

3.3.2.1. Analysis histogram of enzyme-ligand Interactions

The target Compound 2 revealed increased stability with **HDAC-2** in comparison to the interactions with **HDAC-8**. Compound 2 showed a notable binding pattern within the active pocket of **HDAC-2**. It formed π -interactions with the subsequent residues: Phe155 (~22%), His183 (~15%), Phe210 (~25%), Leu276 (~15%), and Tyr308 (~40%), as presented in **Figure 17 A-B**. Additionally, Compound 2 interacted with **HDAC-2** by some H-bonds with residues, Asp104 (~60%), Gly143 (~80%), His145 (~95%), His146 (~90%), Asp181 (~80%), Gly267 (~170%), Asp269 (~110%), Gly304 (~90%), Gly304 (~30%), and Tyr308 (~60%) **Figure 17A-B**. Another type of hydrogen bond interaction is the water-bridged hydrogen bond, where water molecules from the crystal structure create a connection between the enzyme residues and ligands. Furthermore, Compound 2 was capable of forming ionic bonds with the residues Asp181 (~10%), Asp269 (~5%), and ZN metal when complexed with HDAC-2.

On the other hand, Compound 2 formed H-bond interactions with the following residues: Lys33 (~20%), Asp101 (~175%), and Asp267 (~30%), as presented in **Figure 17c-d**. Additionally, Compound 2 able to form many hydrogen bonds Hb water bridge and ionic interactions **with HDAC-8**.

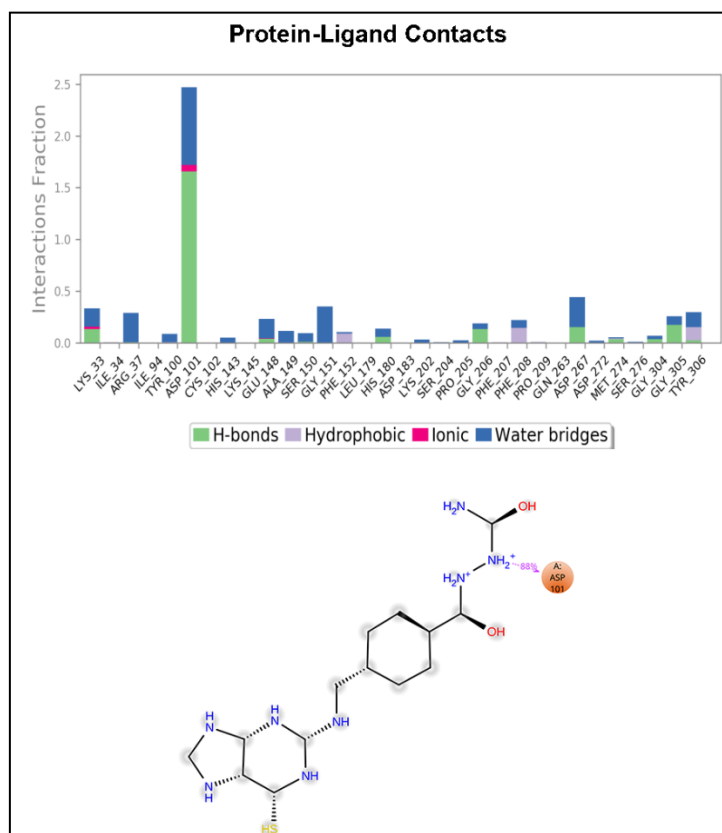
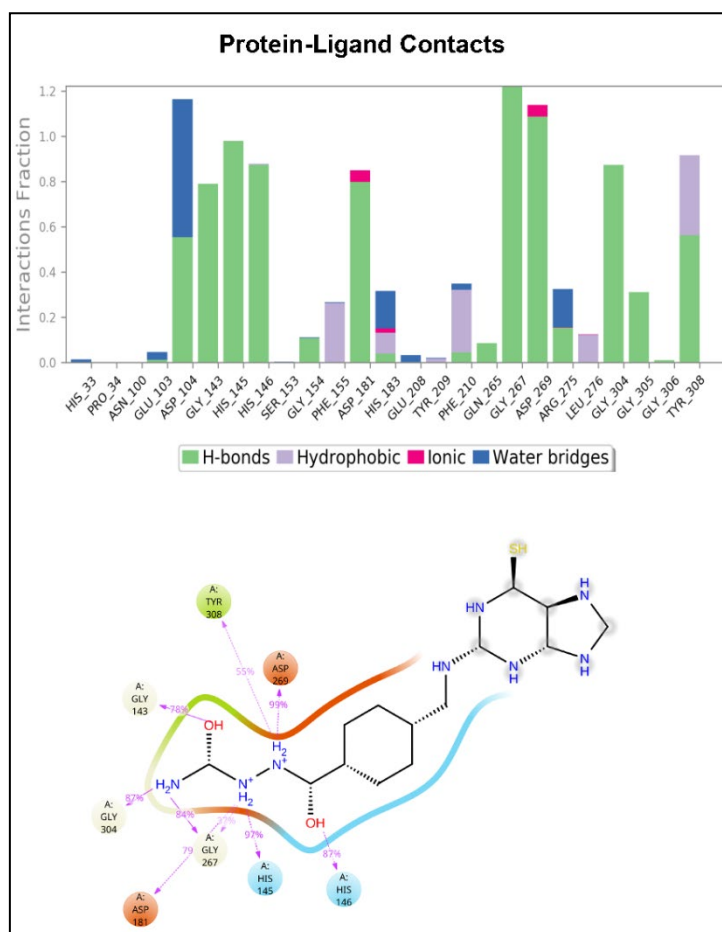


Figure 17. Description of Compound 2 binding with HDAC-2 (A-B) and HDAC-8 (C-D) during the 100 ns simulation period.

Another approach to monitoring these interactions involves plotting the number of interactions over time using a heatmap (**Figures 18 and 19**) that represents the interaction count at each frame of Compound 2 with HDAC-2 and HDAC-8. In contrast, the dark colour represents a greater number of interactions. Based on the heat map figures, it was noted that the protein exhibited the highest number of conformations of HDAC-2 and HDAC-8, forming up to nine and four hydrogen bonds for each complex, respectively. The most interacted amino acids of HDAC-2 with Compound 2 are Asp104, Gly143, His146, His145, Asp181, Gly267, Asp269, and Tyr308. Additionally, the most shared amino acids interactions of Compound 2 with HDAC-8 are Asp101, Gly151, Asp267 and Tyr306.

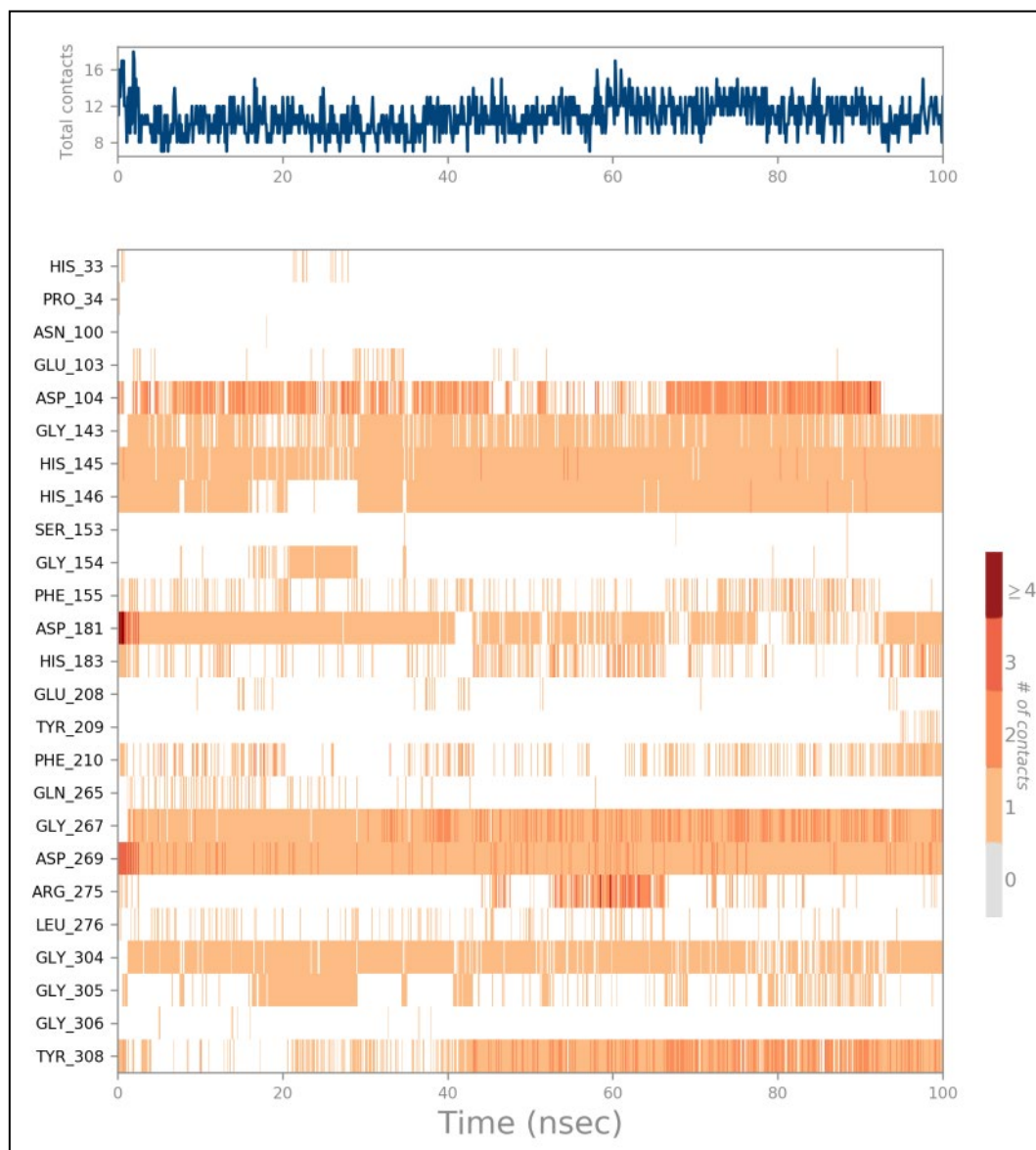


Figure 18. Compound 2-HDAC-2 complex heat map during 100 ns simulation period.

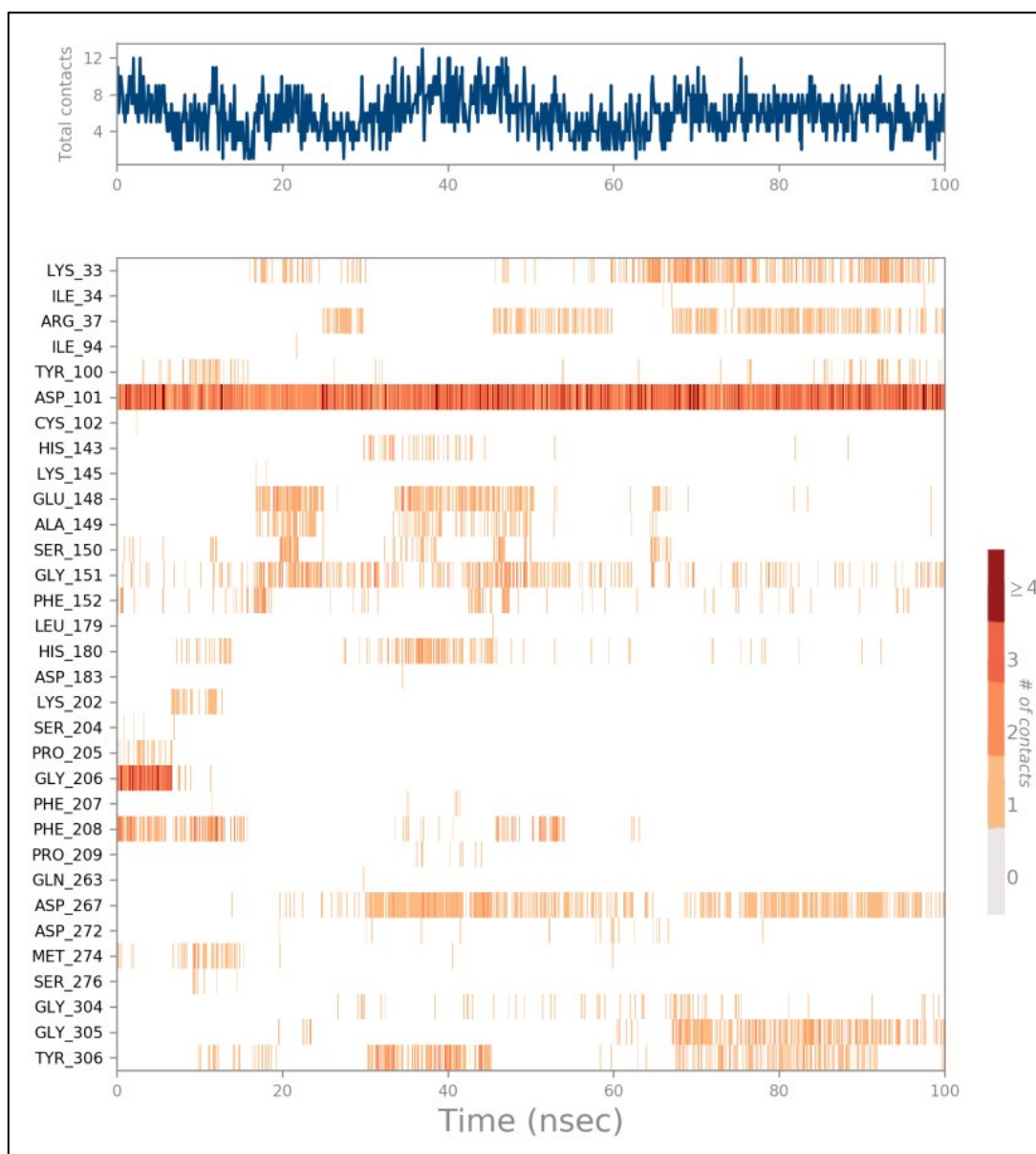


Figure 19. Compound 5-HDAC-8 complex heat map during 100 ns simulation period.

4. Discussion

The binding interactions of various compounds with **HDAC-2** and **HDAC-8** were evaluated to understand their potential activity. The simulation focused on the affinity scores, hydrophobic π -interactions, hydrogen bonds, and metal ionic interactions that stabilize the binding compounds in the site of action. The compounds studied displayed a range of binding affinities for **HDAC-2** and **HDAC-8**; all compounds showed considerable results but Compound 2 exhibited the strongest binding to HDAC-2 (-8.13 kcal/mol), and Compound 3 showed the highest affinity for **HDAC-8** (-7.93 kcal/mol). The interaction profiles were characterized by a combination of hydrophobic π -interactions, hydrogen bonds, and metal ionic interactions, particularly with **Zn401** for HDAC-2 and **Zn378** for HDAC-8. These interactions suggest that metal coordination is crucial for the stability of the inhibitor-enzyme complex, with hydrophobic interactions playing an important role in the binding specificity. The reference drugs, **SAHA** and **Trichostatin**, provided valuable benchmarks for evaluating the potential of these compounds as HDAC inhibitors. The best result from the above work is the interaction of **Compound 2** with **HDAC-2**, which showed the highest binding affinity score of **-8.13 kcal/mol**. although

these results are preliminary they represent a motivation for chemical synthesis and purification of the tested derivative and going further tests.

5. Conclusion

Compound 2 represents the best result from this work due to its high binding affinity, extensive interaction network, and competitive performance against reference drugs. The combination of hydrophobic π -interactions, hydrogen bonds, and metal ion coordination suggests that **Compound 2** could be a potent **HDAC-2** inhibitor, making it an excellent candidate for further experimental validation and potential therapeutic development. to conform these results after the synthesis and purification of the selected compound in-vitro enzymatic inhibitor activity is required than cytotoxic, selectivity and overall therapeutic potential to be tested.

Author contributions

Conceptualization, Ameer H. Alwash and Shymaa A. Husein ; methodology, Saraa M. Harbi; software, Mustafa M. Mukhlif; validation, Mustafa M. Mukhlif, and Ameer H. Alwash; formal analysis, ; investigation, Mustafa M. Mukhlif; resources, Mohammed Khalid Abbood; visualization, Mustafa M. Mukhlif; supervision, Ameer H. Alwash; project administration, Hind A. Yaseen; funding acquisition, Mohammed Khalid Abbood. All authors have read and agreed to the published version of the manuscript.

Funding

Research has not received any external funding.

Acknowledgments

The authors are truly grateful to Al-Bayan University and the College of Pharmacy for their support.

Conflict of interest

The authors declare no conflict of interest.

References

1. Khatami F, Bahri RA, Sharifkazemi H, Sajadi SM, Shamshirgaran A, Le Calvez-Kelm F. Molecular biology and epigenetic modifications definition. In: Genetics and Epigenetics of Genitourinary Diseases. Elsevier; 2025. pp. 37–61.
2. Ilango S, Paital B, Jayachandran P, Padma PR, Nirmaladevi R. Epigenetic alterations in cancer. *Front Biosci-Landmark* 2020; 25: 1058–1109.
3. Esteller M, Dawson MA, Kadoch C, Rassool FV, Jones PA, Baylin SB. The epigenetic hallmarks of cancer. *Cancer Discov* 2024; 14: 1783–1809.
4. Saeed AM, Al-Hamashi AAA. Molecular docking, ADMET study, synthesis, characterization and preliminary antiproliferative activity of potential histone deacetylase inhibitors with isoxazole as new zinc binding group. *Iraqi J Pharm Sci* 2023; 32: 188–203.
5. Al-Amily D, Mohammed MH. Design, synthesis and cytotoxicity study of primary amides as histone deacetylase inhibitors. *Iraqi J Pharm Sci* 2019; 28: 151–158.
6. Rashid MS. Analysis of the Role of Glycogen Synthase Kinase 3 in the Mitotic Checkpoint [PhD thesis]. 2018.
7. Foundation N. Autobiography of Gertrude B. Elion, The Nobel Prize in Physiology or Medicine 1988. *The Oncologist* 2006; 11: 966–968.
8. Peters G, Beijnen J. Purine and pyrimidine metabolism: still a black box? *Pharm World Sci* 1994; 16: 37–39.
9. Elion GB. The purine path to chemotherapy. *Biosci Rep* 1989; 9: 509–529.
10. Munshi PN, Lubin M, Bertino JR. 6-thioguanine: a drug with unrealized potential for cancer therapy. *The Oncologist* 2014; 19: 760–765.
11. Dubinsky MC, Hassard PV, Seidman EG, Kam LY, Abreu MT, Targan SR, Vasilias EA. An open-label pilot study using thioguanine as a therapeutic alternative in Crohn's disease patients resistant to 6-mercaptopurine therapy. *Inflamm Bowel Dis* 2001; 7: 181–189.

12. van den Brand FF, van Nieuwkerk CM, Verwer BJ, de Boer YS, de Boer NK, Mulder CJ, Bloemena E, Bakker CM, Vrolijk JM, Drenth JP. Biochemical efficacy of tioguanine in autoimmune hepatitis: a retrospective review of practice in the Netherlands. *Aliment Pharmacol Ther* 2018; 48: 761–767.
13. Tack G, Van Asseldonk D, Van Wanrooij R, Van Bodegraven A, Mulder C. Tioguanine in the treatment of refractory coeliac disease—a single centre experience. *Aliment Pharmacol Ther* 2012; 36: 274–281.
14. van Gils T, van de Donk T, Bouma G, van Delft F, Neeffjes-Borst EA, Mulder CJ. The first cases of collagenous sprue successfully treated with thioguanine. *BMJ Open Gastroenterol* 2016; 3: e000099.
15. Demis DJ, Brown CS, Crosby WH. Thioguanine in the treatment of certain autoimmune, immunologic and related diseases. *Am J Med* 1964; 37: 195–205.
16. Heraiz AA, Abdelwahab MF, Saleh AM, Ragab EA, Eldondaity SA. Antidiabetic activity of *Ipomoea cairica* (L.) Sweet leaves: in-vitro and in-silico antidiabetic potential of isolated flavonoid glycosides and sulphated flavonoids. *Nat Prod Res* 2023; 37: 4251–4255.
17. Saleh AM, Mahdy HA, El-Zahabi MA, Mehany AB, Khalifa MM, Eissa IH. Design, synthesis, in silico studies, and biological evaluation of novel pyrimidine-5-carbonitrile derivatives as potential anti-proliferative agents, VEGFR-2 inhibitors and apoptotic inducers. *RSC Adv* 2023; 13: 22122–22147.
18. El Azab EF, Alakilli SY, Saleh AM, Alhassan HH, Alanazi HH, Ghanem HB, Yousif SO, Alrub HA, Anber N, Elfaki EM. *Actinidia deliciosa* extract as a promising supplemental agent for hepatic and renal complication-associated type 2 diabetes (in vivo and in silico-based studies). *Int J Mol Sci* 2023; 24: 13759.
19. Kumar BK, Faheem N, Sekhar KVG, Ojha R, Prajapati VK, Pai A, Murugesan S. Pharmacophore-based virtual screening, molecular docking, molecular dynamics and MM-GBSA approach for identification of prospective SARS-CoV-2 inhibitor from natural product databases. *J Biomol Struct Dyn* 2022; 40: 1363–1386.
20. Ivanova L, Tammiku-Taul J, García-Sosa AT, Sidorova Y, Saarma M, Karelson M. Molecular dynamics simulations of the interactions between glial cell line-derived neurotrophic factor family receptor GFR α 1 and small-molecule ligands. *ACS Omega* 2018; 3: 11407–11414.